52 $Cu(HCOO)_2 \cdot 4H_2O$

52A Pure compound

No. 52A-1 $Cu(HCOO)_2 \cdot 4H_2O$, Cupric formate tetrahydrate

(M = 225.642; [D: 235.70])

1a Antiferroelectric activity of $Cu(HCOO)_2 \cdot 4H_2O$ was first reported by Okada in 1965. 65Oka
Antiferromagnetic activity of $Cu(HCOO)_2 \cdot 4H_2O$ was reported independently by Itoh et al. in 1962 and Kobayashi et al. in 1963. 62Ito, 63Kob

b

phase	III [c])	II [a])	I [a])
state	A [b]), A_{magn}*) [c])	A [b]), P_{magn} [c])	P [b]), P_{magn} [c])
crystal system			monoclinic [d])
space group			$P2_1/a - C_{2h}^5$ [d])
Θ [K]	17		235.5 [a])

[a]) 62Kir1
[b]) 65Oka
[c]) 63Kob, 62Ito
[d]) 54Kir
[e]) 67Oka
[f]) 71Bir
[g]) 69Sod
[h]) 73Mak

For the deuterated crystal, Θ_{II-I} = 245.7 K [e]).
Two different assignments were proposed for the space group of phase II (monoclinic): $P2_1$ [f]) and $P2_1/n$ [g]) [h]).
Antiferroelectric axis || [010]. 65Oka
Transparent, blue. Cleavage plane: (001). 54Kir
Efflorescent. 54Kir
*) The antiferromagnetic phase below 17 K is accompanied by weak ferromagnetism. 63Kob

2a Crystal growth: evaporation or cooling method from aqueous solution. 65Oka
b Crystal form: Fig. 52A-1-001.

3a Unit cell parameters: a = 8.18(2) Å, b = 8.15(2) Å, c = 6.35(2) Å, β = 101° 5(20)′ at RT. 54Kir
b Z = 2 in phase I [a]), Z = 4 in phase II [b]). [a]) 54Kir [b]) 72Kay

Crystal structure: positional and temperature parameters: Table 52A-1-001, Table 52A-1-002.
Bond lengths and bond angles: Table 52A-1-003, Table 52A-1-004.
Projection of crystal structure: Fig. 52A-1-002, Fig. 52A-1-003, Fig. 52A-1-004.
An approximate structure of phase II has been determined by neutron diffraction technique on the assumption that the space group is $P2_1/n$. 72Kay, 67Tub
The crystal has a super-structure with the c axis doubled in phase II.

4 Thermal expansion: Fig. 52A-1-005.

5a Dielectric constant: Fig. 52A-1-006, Fig. 52A-1-007.
Dielectric relaxation: Fig. 52A-1-008, Fig. 52A-1-009, Fig. 52A-1-010.
$\kappa_b = C/(T - \Theta_p)$, where $C = 3.2 \cdot 10^4$ K, Θ_p = 215 K. 65Oka
Phase diagram with regard to p: Fig. 52A-1-011.
b Nonlinear dielectric properties: Fig. 52A-1-012, Fig. 52A-1-013, Fig. 52A-1-014, Fig. 52A-1-015.

6a	Heat capacity: Fig. 52A-1-016, Fig. 52A-1-017, Fig. 52A-1-018, Fig. 52A-1-019.	
	Transition heat and transition entropy:	
	$\Delta Q_m = 836.0(10)$ J mol^{-1}, $\Delta S_m = 3.546(5)$ J K^{-1} mol^{-1}.	76Mat
	For $Cu(HCOO)_2 \cdot 4D_2O$: $\Delta Q_m = 936.9(5)$ J mol^{-1}, $\Delta S_m = 3.814(2)$ J K^{-1} mol^{-1}.	76Mat
b	Thermal conductivity: Fig. 52A-1-020.	
8a	Elastic compliance and stiffness: Table 52A-1-005; Fig. 52A-1-021, Fig. 52A-1-022.	
9a	Birefringence: Fig. 52A-1-023, Fig. 52A-1-024.	
10a	Raman scattering: Fig. 52A-1-025.	
11	Electrical conduction: Fig. 52A-1-026.	
	Protonic conductivity parallel to the water planes (perpendicular to (110)):	75Web
	$\sigma = 4.5(13) \cdot 10^{-15}$ Ω^{-1} m^{-1} at RT.	
	Activation energy: $\Delta U = 54.5$ kJ mol^{-1} ($T > \Theta_a$), $\Delta U = 63.5$ kJ mol^{-1} ($T < \Theta_a$).	75Web
	Protonic conductivity perpendicular to the water layer is small:	75Web
	$\sigma_c \approx 10^{-6}$ Ω^{-1} m^{-1} at RT.	
	Ohmic conductivity at 298 K (protonic): $\sigma_a = 8.5(21) \cdot 10^{-6}$ Ω^{-1} m^{-1};	77Mur
	$\sigma_b = 5.5(16) \cdot 10^{-5}$ Ω^{-1} m^{-1}; $\sigma_c = 7(2) \cdot 10^{-6}$ Ω^{-1} m^{-1}.	
	Ohmic and non-ohmic behaviors have been found; for details see	77Mur
12	Magnetic properties: Fig. 52A-1-027, Fig. 52A-1-028, Fig. 52A-1-029, Fig. 52A-1-030.	
	$\Theta_N = 17$ K.	63Kob
13a	NMR: Table 52A-1-006, Table 52A-1-007, Table 52A-1-008, Table 52A-1-009;	
	Fig. 52A-1-031, Fig. 52A-1-032, Fig. 52A-1-033, Fig. 52A-1-034.	
	Proton magnetic resonance at 4.2 K [for $Cu(HCOO)_2 \cdot 4D_2O$]: see	62Kir2, 74Mas
b	ESR: see	68See

Table 52A-1-001. $Cu(HCOO)_2 \cdot 4H_2O$. Crystal structure of phase I [54Kir, 66Oka]. Fractional coordinates and temperature parameters. *B* is defined by Eq. (e) in Introduction.

		[54Kir] X-ray	[66Oka] Neutron diffraction
Cu	*x*	0	0
	y	0	0
	z	0	0
	B	1.35 Å^2	1.02(14) Å^2
C	*x*	0.238	0.237(1)
	y	0.270	0.269(1)
	z	0.018	0.024(1)
	B	1.35 Å^2	1.04(16) Å^2
$O_F(1)$ [1])	*x*	0.206	0.205(1)
	y	–0.092	–0.092(1)
	z	–0.080	–0.080(1)
	B	1.35 Å^2	1.27(16) Å^2
$O_F(2)$ [1])	*x*	0.117	0.116(1)
	y	0.210	0.213(1)
	z	0.086	0.088(1)
	B	1.35 Å^2	1.34(1) Å^2
$O_W(1)$ [1])	*x*	0.423	0.430(2)
	y	0.399	0.401(2)
	z	0.647	0.641(2)
	B	1.35 Å^2	1.94(2) Å^2
$O_W(2)$ [1])	*x*	0.086	0.089(2)
	y	0.349	0.357(2)
	z	0.483	0.482(2)
	B	1.35 Å^2	2.59(22) Å^2

[1]) O_F: O belonging to formate. O_W: O belonging to water. Figures in parentheses correspond to those given in Fig. 52A-1-002.

Table 52A-1-002. $Cu(HCOO)_2 \cdot 4H_2O$. Crystal structure of phase I [75Kay]. Fractional coordinates and temperature parameters. The temperature parameters are defined by Eq. (b) in Introduction.

Atom	x	y	z	b_{11}	b_{22}	b_{33}	b_{12}	b_{13}	b_{23}
				$[10^{-4}]$					
Copper-Cu	0	0	0	35(2)	27(2)	129(4)	1(2)	28(2)	–6(2)
Formate ion									
Carbon C	0.2387(1)	0.2695(2)	0.0244(2)	54(2)	45(2)	144(4)	–7(2)	37(2)	–6(2)
Oxygens OF-1	0.2024(2)	–0.0921(2)	–0.0794(2)	55(2)	40(2)	198(5)	14(2)	50(2)	19(3)
OF-2	0.1145(2)	0.2119(2)	0.0896(2)	62(2)	52(2)	183(5)	–23(2)	55(2)	–23(3)
Hydrogen H_F	0.2037(4)	0.6933(4)	0.0826(6)	190(6)	127(5)	457(13)	70(5)	207(7)	106(6)
Water molecules									
OW-1	0.4287(6)	0.4006(4)	0.6381(4)	98(5)	94(5)	156(8)	–10(5)	36(5)	–17(5)
OW-2	0.0890(5)	0.3596(4)	0.4849(6)	118(9)	110(8)	202(10)	–12(7)	55(8)	–29(8)
H-1	0.3107(13)	0.3920(6)	0.5847(8)	100(8)	142(8)	200(15)	–16(11)	10(10)	–8(8)
H-2	0.4810(12)	0.2978(14)	0.5979(14)	135(16)	136(19)	281(27)	2(13)	20(13)	21(16)
H-3	0.4746(10)	0.4739(8)	0.5424(11)	188(23)	103(21)	210(43)	–20(17)	41(18)	52(18)
H-4	0.0880(4)	0.3257(4)	0.3394(8)	149(6)	171(7)	242(11)	–12(4)	53(7)	–29(8)
H-5	0.0265(12)	0.4587(9)	0.4907(18)	136(39)	111(36)	307(28)	8(24)	51(25)	33(42)
H-6	0.2154(69)	0.3782(35)	0.5355(50)	86(52)	157(50)	288(83)	12(71)	–34(66)	–22(47)
H-7	0.0330(18)	0.2753(28)	0.5438(25)	129(32)	132(35)	306(48)	–47(21)	89(25)	3(30)

Occupancy parameters f_i for the hydrogen site H-i in the water molecules are assumed as below. $f_1 = 0.85, f_2 = 1.5 - f_1, f_3 = 0.5, f_4 = 1.0, f_5 = 0.5, f_6 = 1 - f_1, f_7 = f_1 - 0.5$.
For the hydrogen sites, see Fig. 52A-1-003, Fig. 52A-1-004. See also Fig. 52A-1-002. H_F: H belonging to formate.

Table 52A-1-003. $Cu(HCOO)_2 \cdot 4H_2O$. Crystal structure of phase I [75Kay]. Interatomic distances and angles. "Riding correction" is given in brackets for O–H distances. See also Fig. 52A-1-003, Fig. 52A-1-004. Primed atoms are related to unprimed atoms by symmetry operations.

Bond		Distances [Å]	Bond	Bond angles [°]
Copper octahedron:	Cu–OF(1)	1.970(4)	OF(1)–Cu–OF(2)	91.8(2)
	Cu–OF(2)	1.994(4)	OF(1)–Cu–OW(1)	93.2(2)
	Cu–OW(1)	2.401(7)	OW(1)–Cu–OW(1)	86.8(2)
Formate ion:	C–OF(1)	1.250(3)	OF(1)–C–OF(2)	122.5(2)
	C–OF(2)	1.259(3)	HF–C–OF(1)	119.8(2)
	C–HF	1.093(4) [1.142]	HF–C–OF(2)	117.7(2)
Water-1:	OW(1)–H(1)	0.96(1) [0.98]	H(1)–OW(1)–H(2)	107.4(5)
	OW(1)–H(2)	1.00(2) [1.01]	H(1)–OW(1)–H(3)	107.7(6)
	OW(1)–H(3)	0.98(1) [1.00]	H(2)–OW(1)–H(3)	96.9(8)
Water-2:	OW(2)–H(4)	0.96(1) [0.98]	H(4)–OW(2)–H(5)	104.8(9)
	OW(2)–H(5)	0.96(1) [0.97]	H(4)–OW(2)–H(6)	111.8(8)
	OW(2)–H(6)	1.03(6) [1.05]	H(4)–OW(2)–H(7)	99.5(15)
	OW(2)–H(7)	0.94(3) [0.96]		
Hydrogen bonds:			H(1)–OW(1)---H(3)'	110.2(4)
			H(1)–OW(1)---H(7)	109.1(5)
			H(2)–OW(1)---H(6)	105.2(10)
			H(2)–OW(1)---H(3)'	92.9(6)
			H(3)–OW(1)---H(6)	107.8(11)
			H(3)–OW(1)---H(7)	91.0(6)
			H(6)–OW(1)---H(3)'	110.2(9)
			H(6)–OW(1)---H(7)	106.9(9)
			H(3)'–OW(1)---H(7)	87.0(4)
			H(4)–OW(2)---H(2)	105.4(4)
			H(4)–OW(2)---H(1)	101.5(4)
			H(4)–OW(2)---H(5)	114.6(5)
			H(5)–OW(2)---H(1)	111.6(8)
			H(5)–OW(2)---H(2)	106.3(7)
			H(6)–OW(2)---H(1)	121.6(16)
			H(6)–OW(2)---H(5)'	111.5(16)
			H(7)–OW(2)---H(5)'	105.4(7)
			H(7)–OW(2)---H(1)	119.7(8)
	OW(2)–OF(2)	2.828(8)	OW(2)–H(4)–OF(2)	165.3(3)
	H(4)–OF(2)	1.886(7)		
	OW(1)–OW(1)	2.801(8)	OW(1)–H(3)–OW(1)	175.8(7)
	H(3)–OW(1)	1.826(6)		
	OW(2)–OW(2)	2.739(8)	OW(2)–H(5)–OW(2)	177.2(10)
	H(5)–OW(2)	1.779(6)		
	OW(1)–OW(2)	2.782(8)	OW(1)–H(1)–OW(2)	175.9(4)
	H(1)–OW(2)	1.822(14)	OW(1)–H(6)–OW(2)	175.7(24)
	H(6)–OW(2)	1.751(60)		
	OW(1)–OW(2)	2.767(7)	OW(1)–H(2)–OW(2)	167.9(6)
	H(2)–OW(2)	1.785(19)	OW(1)–H(7)–OW(2)	174.6(11)
	H(7)–OW(1)	1.827(31)		
			H(1)---OW(2)---H(2)	120.1(4)
			H(3)'---OW(2)---H(2)	104.5(4)
			H(5)'–OW(2)---H(1)	111.0(4)
			H(1)---OW(1)---Cu	113.9(4)
			H(2)---OW(1)---Cu	119.5(4)
			H(3)---OW(1)---Cu	109.7(6)

Table 52A-1-004. $Cu(HCOO)_2 \cdot 4H_2O$. Crystal structure of phase I [75Kay]. Root-mean-square amplitudes of thermal motion of hydrogens along the principal axes and angles between the axes and O–O hydrogen bonds.

Atom	Amplitude	Angle [deg]
H–1	0.172(9)	14(10)
	0.206(6)	81(11)
	0.223(6)	79(12)
H–2	0.204(15)	51
	0.213(8)	80(30)
	0.245(14)	41(13)
H–3	0.149(25)	22(8)
	0.225(8)	87(9)
	0.254(14)	69(8)
H–4	0.205(5)	20(18)
	0.218(4)	71(18)
	0.250(5)	89(6)
H–5	0.186(28)	37(42)
	0.208(30)	58(50)
	0.252(20)	73(25)
H–6	0.152(50)	14(30)
	0.224(34)	85(41)
	0.268(36)	77(24)
H–7	0.148(29)	19(15)
	0.231(14)	79(15)
	0.258(16)	75(15)

Table 52A-1-005. $Cu(HCOO)_2 \cdot 4H_2O$. Elastic stiffness [$\cdot 10^{10}$ N m^{-2}] at room temperature [73Kam].

c_{11} = 4.45	c_{22} = 4.99	c_{33} = 2.11
c_{44} = 0.54	c_{55} = 0.71	c_{66} = 2.35
c_{12} = 3.41	c_{23} = 1.49	c_{13} = 1.42
c_{15} = –0.07	c_{25} = 0.27	c_{35} = –0.29
c_{16} = –0.24		

Table 52A-1-006. $Cu(DCOO)_2 \cdot 4D_2O$. Direction cosines of the principal axes of the field gradient tensors at D of formate ions above (D_F) and below Θ_a [$D_F(1)$ and $D_F(2)$] [69Sod]. $X_c \parallel \boldsymbol{a}$, $Y_c \parallel \boldsymbol{b}$, $Z_c \parallel \boldsymbol{c^*}$.

			X_c	Y_c	Z_c
291 K	D_F	ϕ_{xx}	0.329(84)	∓ 0.495(76)	0.805(14)
		ϕ_{yy}	0.735(36)	± 0.669(55)	0.111(94)
		ϕ_{zz}	–0.593(6)	± 0.555(5)	0.584(7)
153 K	$D_F(1)$	ϕ_{xx}	0.267(172)	∓ 0.544(144)	0.796(41)
		ϕ_{yy}	0.756(60)	± 0.630(123)	0.177(183)
		ϕ_{zz}	–0.598(5)	± 0.555(4)	0.579(6)
	$D_F(2)$	ϕ_{xx}	0.357(192)	∓ 0.507(174)	0.785(25)
		ϕ_{yy}	0.738(92)	± 0.668(131)	0.096(206)
		ϕ_{zz}	–0.573(4)	± 0.545(3)	0.612(4)

Table 52A-1-007. $Cu(DCOO)_2 \cdot 4D_2O$. Principal values and asymmetry parameter η of field gradient tensors at D of formate ion above and below Θ_a [69Sod].

		$eQ\phi_{zz}/h$	$eQ\phi_{yy}/h$	$eQ\phi_{xx}/h$	η
		kHz			
291 K	D_F	155.3(25)	–84.2(29)	–71.0(24)	0.085(24)
253 K	D_F	157.2(19)	–82.7(21)	–74.5(18)	0.053(18)
244 K	$D_F(1)$	157.9(17)	–83.3(21)	–74.8(19)	0.057(16)
	$D_F(2)$	157.2(23)	–82.5(19)	–74.7(17)	0.050(15)
153K	$D_F(1)$	161.4(20)	–83.4(21)	–77.9(34)	0.034(20)
	$D_F(2)$	160.4(17)	–82.1(20)	–78.2(17)	0.025(16)

Table 52A-1-008. $Cu(DCOO)_2 \cdot 4D_2O$. Direction cosines of the principal axes of the field gradient tensors at D of water molecules in phase II at 153 K [69Sod]. $X_c \parallel \boldsymbol{a}$, $Y_c \parallel \boldsymbol{b}$, $Z_c \parallel \boldsymbol{c}^*$. $D_a \ldots D_h$: D at 8 different sites. For numbering of hydrogen atoms, see [66Oka].

		X_c	Y_c	Z_c
D_a	ϕ_{xx}	–0.773(66)	0.327(67)	0.544(133)
D(2)	ϕ_{yy}	0.395(125)	0.424(55)	–0.815(89)
	ϕ_{zz}	–0.497(6)	0.845(3)	0.199(9)
D_c	ϕ_{xx}	–0.243(55)	0.874(84)	0.421(143)
D(1')	ϕ_{yy}	–0.298(41)	–0.480(152)	0.825(74)
	ϕ_{zz}	0.923(3)	0.075(15)	0.377(6)
D_b	ϕ_{xx}	–0.054(64)	0.038(32)	0.998(5)
D(5)	ϕ_{yy}	0.853(5)	–0.519(6)	0.066(71)
	ϕ_{zz}	0.520(5)	0.854(3)	–0.005(10)
D_e	ϕ_{xx}	0.531(127)	0.790(88)	0.308(15)
D(4)	ϕ_{yy}	–0.829(82)	0.560(125)	–0.007(50)
	ϕ_{zz}	–0.178(9)	–0.252(16)	0.951(5)
D_d	ϕ_{xx}	0.279(34)	0.513(111)	–0.812(59)
D(1)	ϕ_{yy}	0.241(36)	–0.856(66)	–0.458(106)
	ϕ_{zz}	–0.930(3)	–0.069(15)	–0.362(7)
D_h	ϕ_{xx}	–0.691(74)	–0.083(110)	–0.715(59)
D(3)	ϕ_{yy}	–0.495(100)	0.776(12)	0.391(104)
	ϕ_{zz}	0.523(6)	0.625(4)	–0.580(6)
D_f	ϕ_{xx}	–0.764(60)	0.645(69)	0.041(34)
D(4')	ϕ_{yy}	0.608(76)	0.696(59)	0.381(18)
	ϕ_{zz}	0.217(13)	0.316(19)	–0.924(7)
D_g	ϕ_{xx}	0.073(61)	0.539(33)	–0.839(26)
D(7)	ϕ_{yy}	–0.828(6)	–0.437(41)	–0.352(62)
	ϕ_{zz}	–0.556(5)	0.721(3)	0.414(7)

Table 52A-1-009. $Cu(DCOO)_2 \cdot 4D_2O$. $|e^2qQ/h|$ and η of D in water molecules in phase II at 153 K. For assignment, see [69Sod]. D_a…D_h: D at 8 different sites.

	$\lvert e^2qQ/h\rvert$ [kHz]	η	Assignment	
D_a	215.5(37)	0.074(20)	D(2)	$>O_{I'}$
D_c	216.6(23)	0.079(27)	D(1')	
D_b	213.6(36)	0.136(21)	D(5)	$>O_{II}$
D_e	220.6(47)	0.091(40)	D(4)	
D_d	214.2(23)	0.104(28)	D(1)	$>O_{I}$
D_h	214.0(32)	0.094(17)	D(3)	
D_f	220.7(43)	0.112(36)	D(4')	$>O_{II'}$
D_g	215.0(33)	0.134(20)	D(7)	

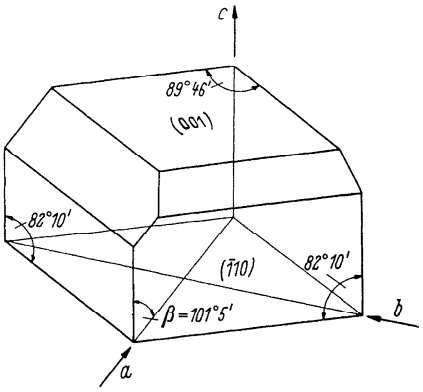

Fig. 52A-1-001. $Cu(HCOO)_2 \cdot 4H_2O$. Crystal form [66Oka].

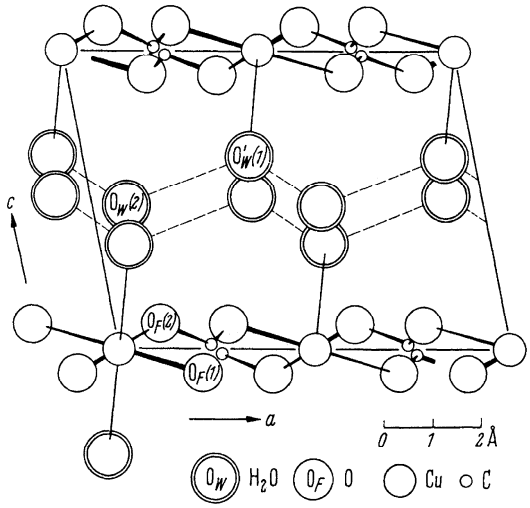

Fig. 52A-1-002. $Cu(HCOO)_2 \cdot 4H_2O$. Crystal structure of phase I [54Kir]. Projection along *b*. Broken lines show the layer of water molecules. O_F: O belonging to formate. O_W: O belonging to water.

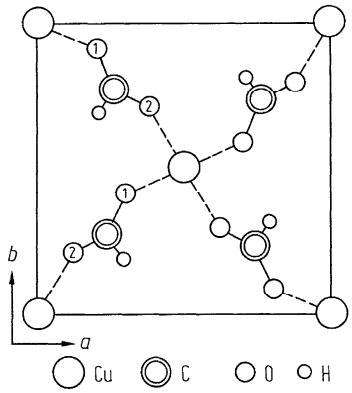

Fig. 52A-1-003. $Cu(HCOO)_2 \cdot 4H_2O$. Crystal structure of phase I [75Kay]. Copper formate layer near $z = 0$.

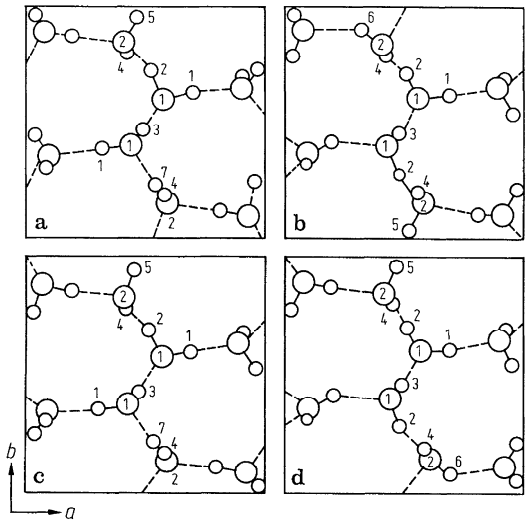

Fig. 52A-1-004. $Cu(HCOO)_2 \cdot 4H_2O$. Crystal structure of phase I [75Kay]. Schematic representation of four possible fully hydrogen bonded water layers. The structures in (**a**) and (**b**) probably make up the water layer in the paraelectric phase, although the same occupancies may be derived from (**c**) and (**d**). (a) and (b) contain 2_1 screw axes and (c) and (d) *a* glide planes. The screw axes are retained through the transition. Large circles denote oxygen atoms, small circles hydrogen atoms.

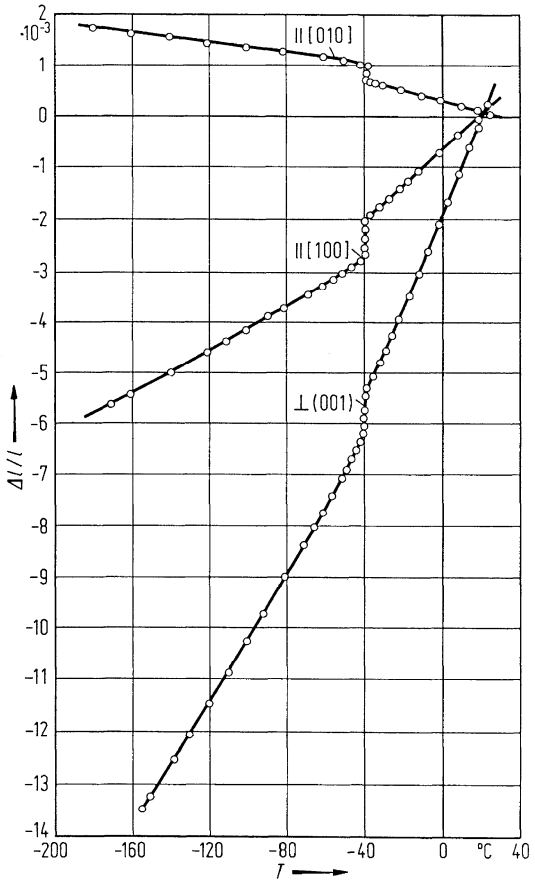

Fig. 52A-1-005. $Cu(HCOO)_2 \cdot 4H_2O$. $\Delta l//l$ vs. $T \parallel$ [100], [010] and $\perp$ (001) [68Seo]. $\Delta l//l$: linear thermal expansion.

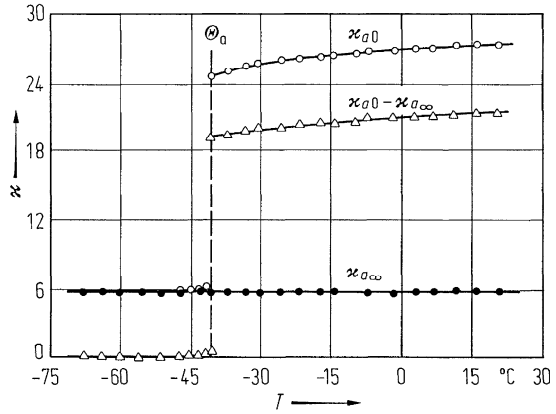

Fig. 52A-1-006. $Cu(HCOO)_2 \cdot 4H_2O$. κ_{a0}, $\kappa_{a\infty}$, $\kappa_{a0} - \kappa_{a\infty}$ vs. T [78Ham]. κ_{a0}, $\kappa_{a\infty}$: dielectric constants along the a axis at static and high-frequency limit, respectively.

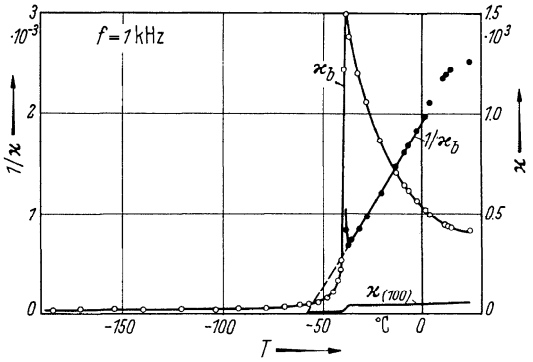

Fig. 52A-1-007. $Cu(HCOO)_2 \cdot 4H_2O$. κ_b, $1/\kappa_b$, $\kappa_{(100)}$ vs. T [65Oka].

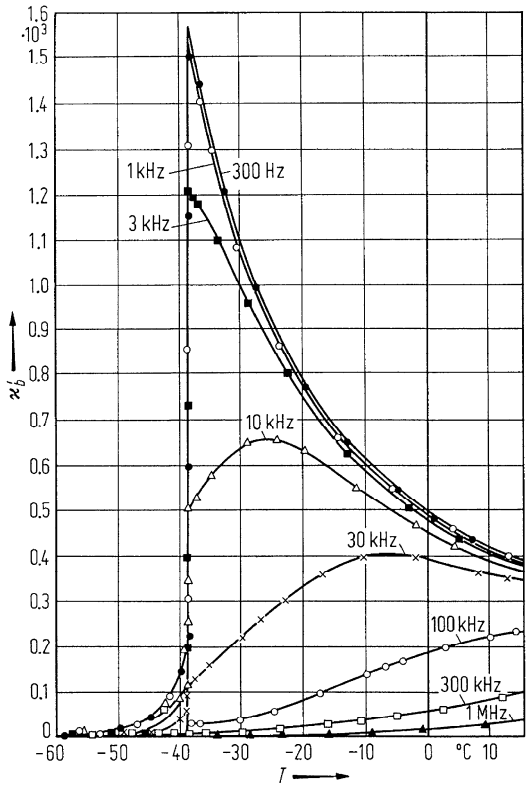

Fig. 52A-1-008. $Cu(HCOO)_2 \cdot 4H_2O$. κ_b' vs. T [69Mak]. Parameter: *f*.

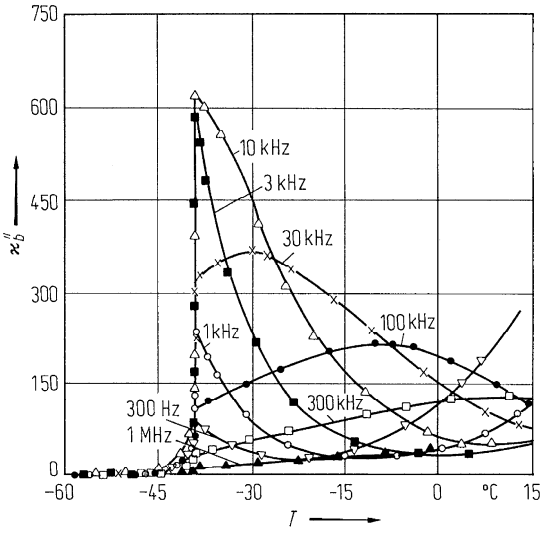

Fig. 52A-1-009. $Cu(HCOO)_2 \cdot 4H_2O$. κ_b'' vs. T [69Mak]. Parameter: *f*.

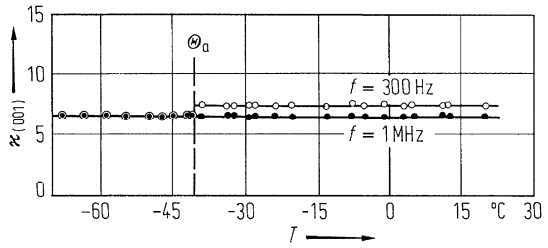

Fig. 52A-1-010. $Cu(HCOO)_2 \cdot 4H_2O$. $\varkappa_{(001)}$ vs. T [78Ham]. Parameter: *f.* $\varkappa_{(001)}$: dielectric constant for $\boldsymbol{E} \perp (001)$.

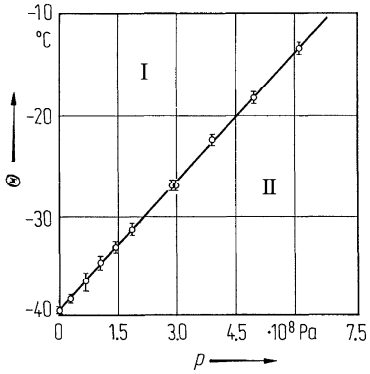

Fig. 52A-1-011. $Cu(HCOO)_2 \cdot 4H_2O$. Θ vs. p [73Ges].

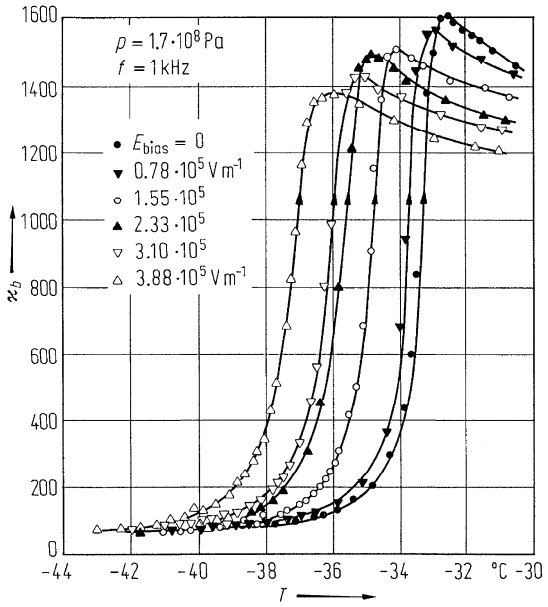

Fig. 52A-1-012. $Cu(HCOO)_2 \cdot 4H_2O$. $\varkappa_b$ vs. T [77Fuj]. Parameter: E_{bias}. $p = 1.7 \cdot 10^8$ Pa.

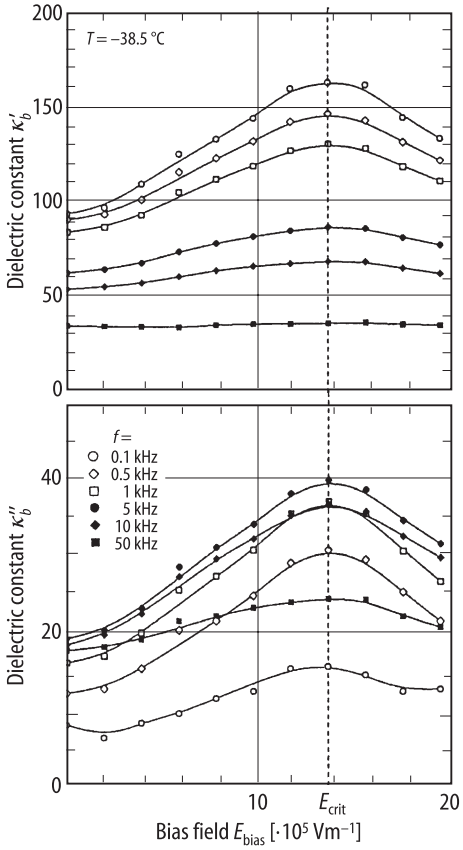

Fig. 52A-1-013. $Cu(HCOO)_2 \cdot 4H_2O$. κ_b', κ_b'' vs. E_{bias} at T = –38.5 °C [92Yas]. Parameter: *f*. E_{crit}: transition field from antiferro- to ferroelectric state.

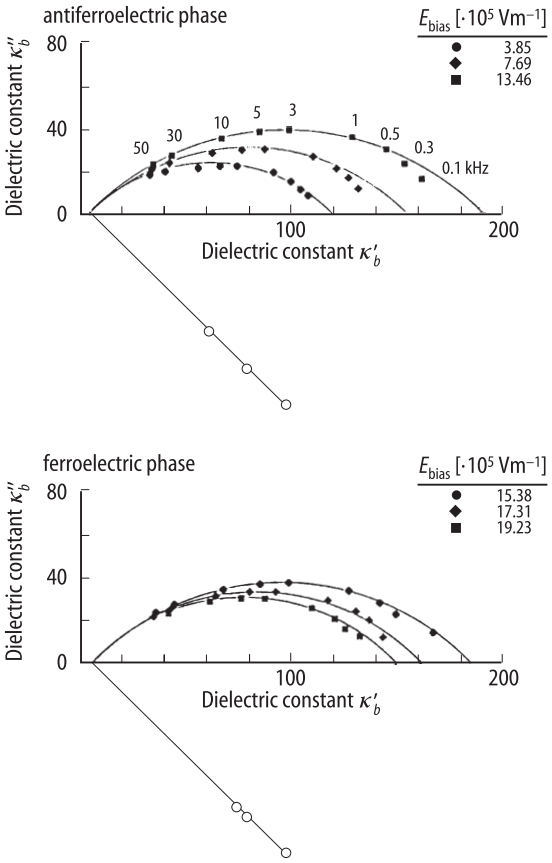

Fig. 52A-1-014. $Cu(HCOO)_2 \cdot 4H_2O$. Cole-Cole diagram of complex dielectric constant [92Yas]. Parameter: E_{bias}. Open circle: center of Cole-Cole arc.

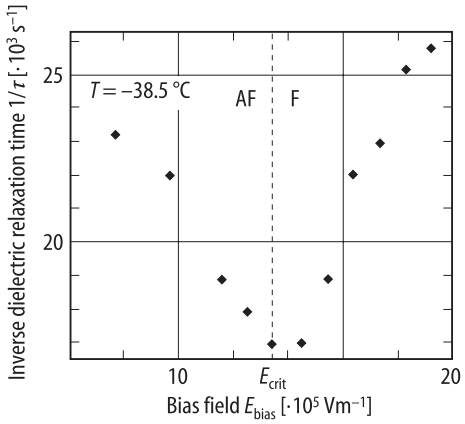

Fig. 52A-1-015. $Cu(HCOO)_2 \cdot 4H_2O$. $1/\tau$ vs. E_{bias} at $T = -38.5$ °C [92Yas]. τ: dielectric relaxation time.

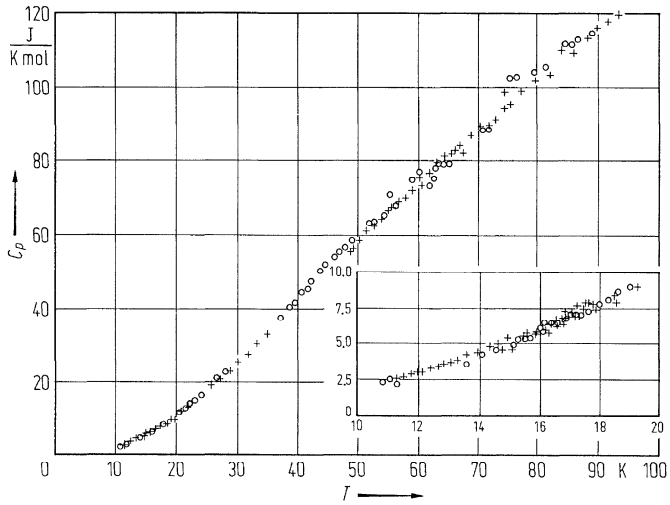

Fig. 52A-1-016. $Cu(HCOO)_2 \cdot 4H_2O$. C_p vs. T near the antiferromagnetic Néel temperature [62Ska]. C_p: molar heat capacity at constant pressure.

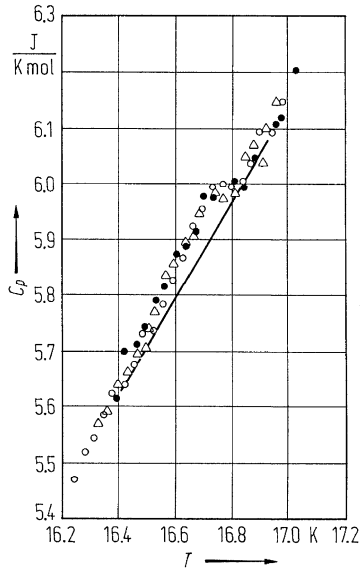

Fig. 52A-1-017. $Cu(HCOO)_2 \cdot 4H_2O$. C_p vs. T [75Yam]. C_p: molar heat capacity at constant pressure. Different symbols correspond to different measurements.

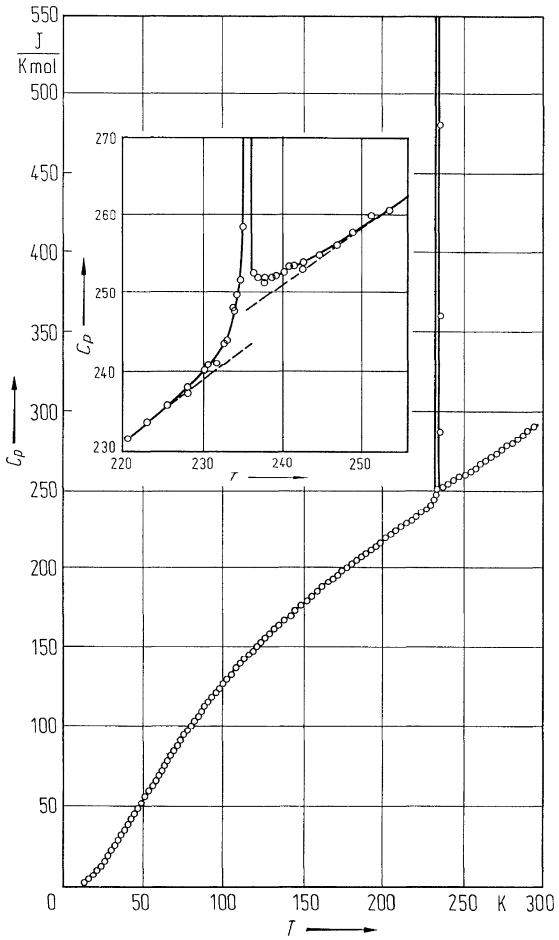

Fig. 52A-1-018. $Cu(HCOO)_2 \cdot 4H_2O$. C_p vs. T [76Mat]. C_p: molar heat capacity at constant pressure.

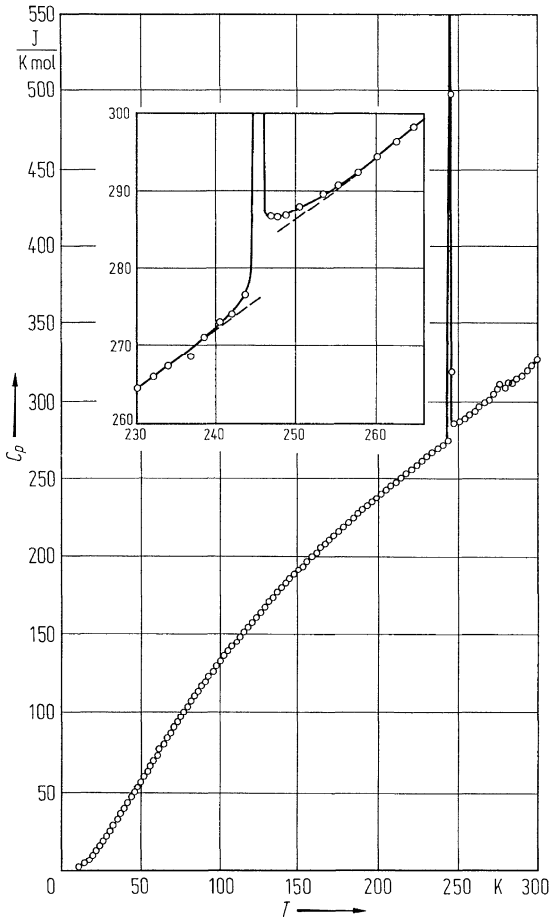

Fig. 52A-1-019. $Cu(HCOO)_2 \cdot 4D_2O$. C_p vs. T [76Mat]. C_p: molar heat capacity at constant pressure.

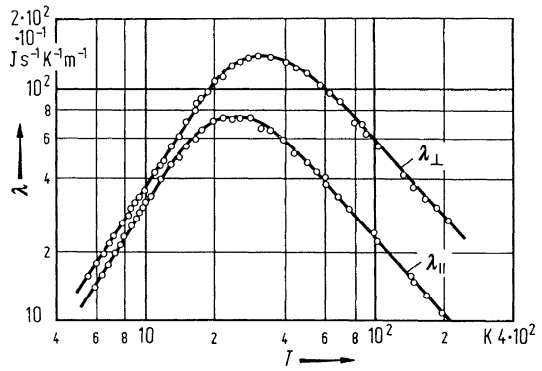

Fig. 52A-1-020. $Cu(HCOO)_2 \cdot 4H_2O$. $\lambda_\perp$, $\lambda_{||}$ vs. T [72Hir]. $\lambda_\perp$, $\lambda_{||}$: thermal conductivity $\perp$ (001), $||$ [001], respectively.

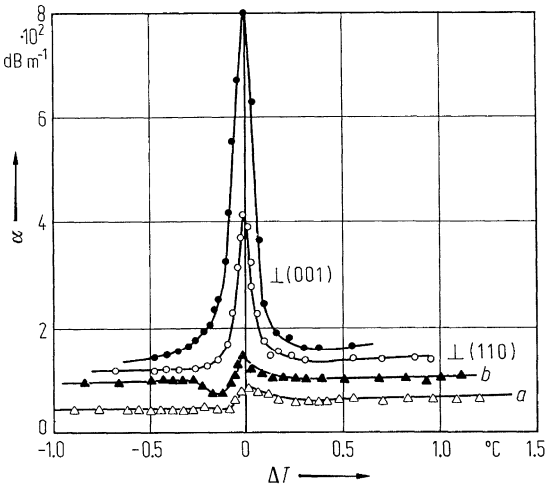

Fig. 52A-1-021. $Cu(HCOO)_2 \cdot 4H_2O$. α vs. ΔT [73Kam]. α: attenuation coefficients for the longitudinal sound wave propagating along the *a* axis, the *b* axis, and $\perp$ to the (110) habit plane and the (001) habit plane. $\Delta T = T - \Theta_a$, $f = 30$ MHz.

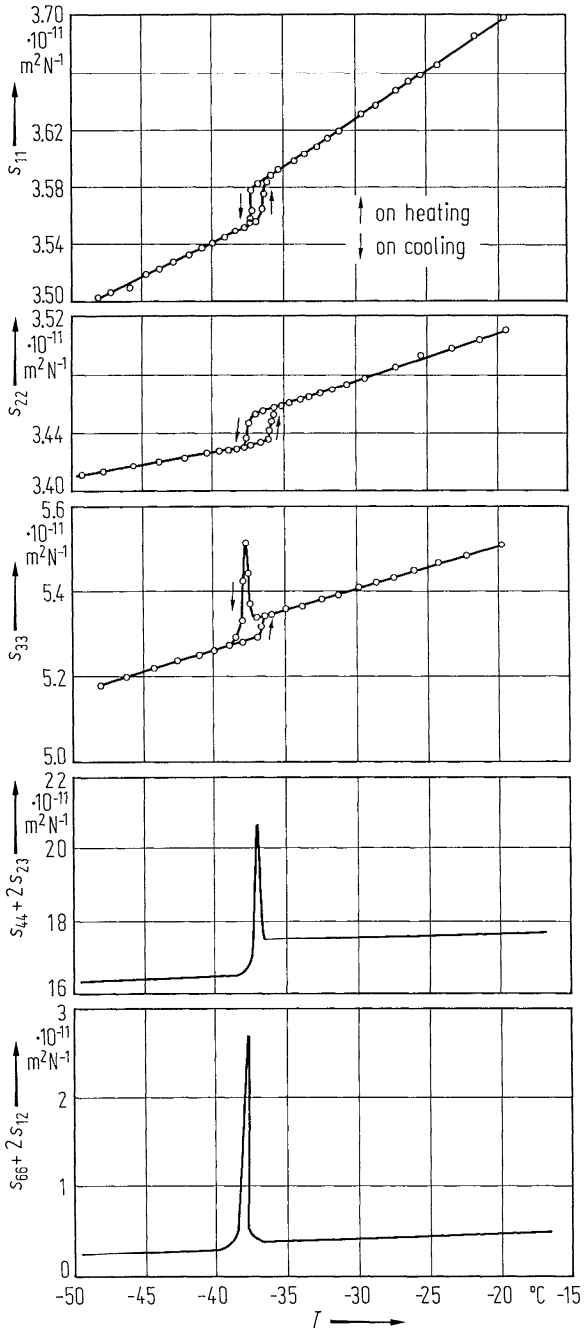

Fig. 52A-1-022. $Cu(HCOO)_2 \cdot 4H_2O$. $s_{\lambda\mu}$ vs. T [74Sas].

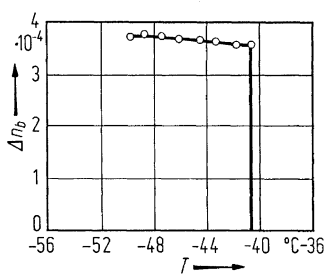

Fig. 52A-1-023. $Cu(HCOO)_2 \cdot 4H_2O$. Δn_b vs. T [70Apk]. $\lambda = 632.8$ nm.

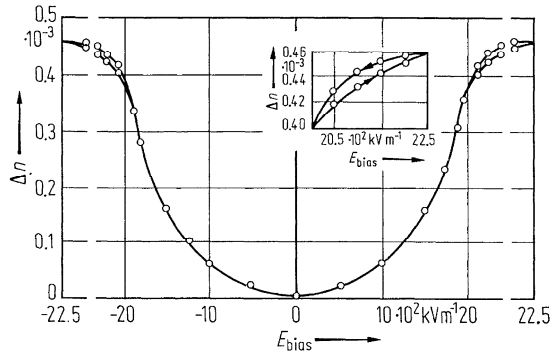

Fig. 52A-1-024. $Cu(HCOO)_2 \cdot 4H_2O$. Δn vs. E_{bias} [70Apk]. $T = -40.5$ °C, $\lambda = 632.8$ nm. The insert indicates an enlarged version of E_{bias} between 20 and $22.5 \cdot 10^2$ kV m^{-1}.

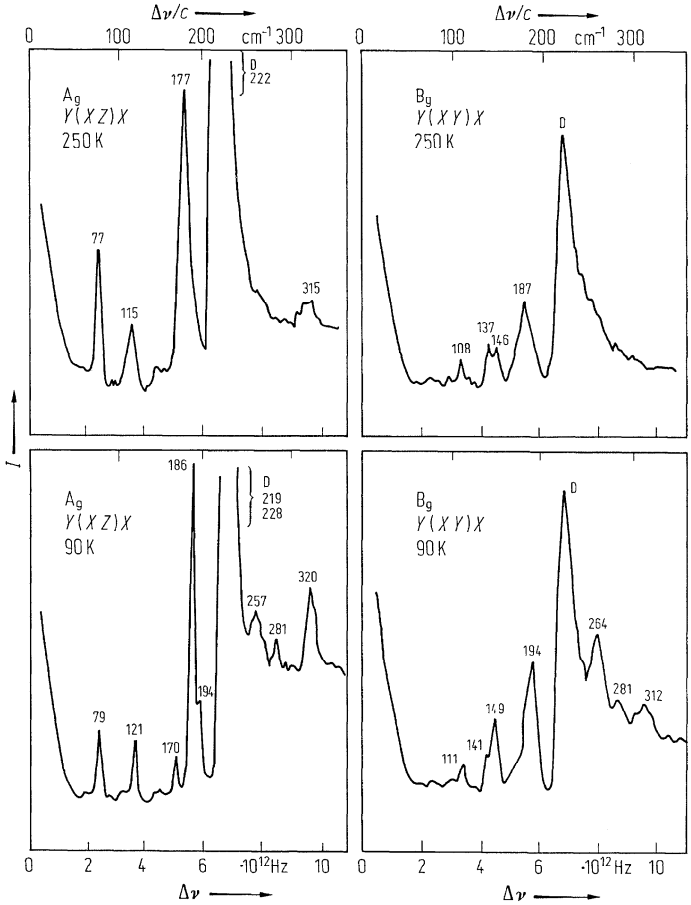

Fig. 52A-1-025. $Cu(HCOO)_2 \cdot 4H_2O$. I vs. $\Delta\nu$ [73Can]. I: Raman scattering intensity for the low frequency region. Upper two spectra are in the paraelectric (250 K), and the lower two are in the antiferroelectric phase (90 K). Peak frequencies are indicated in the figure in units of cm^{-1}. D is a laser discharge line.

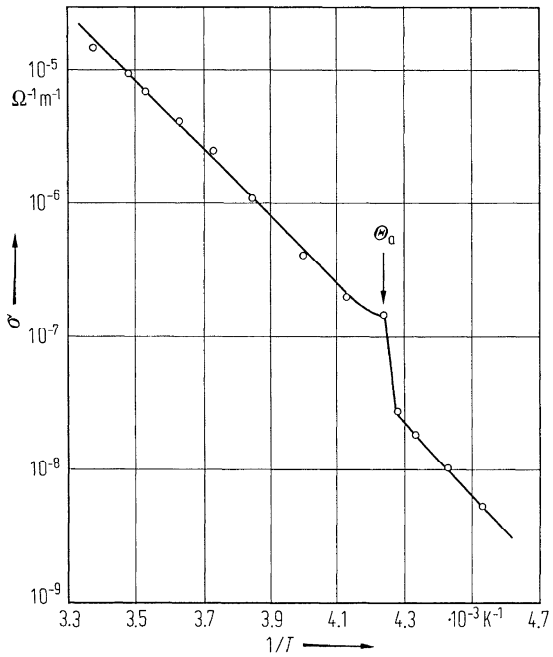

Fig. 52A-1-026. $Cu(HCOO)_2 \cdot 4H_2O$. Protonic dc conductivity σ vs. $1/T$ [75Web]. Electrodes were saturated cupric formate tetrahydrate solutions of diethylene glycol 2-methoxy ethyl ether and distilled water. σ was measured $\perp$ to the naturally occurring (110) face.

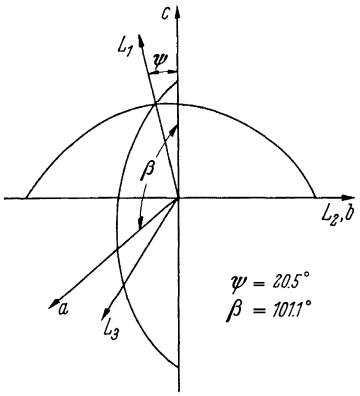

Fig. 52A-1-027. $Cu(HCOO)_2 \cdot 4H_2O$. Relation between the crystallographic axes (*a*, *b*, *c*) and the magnetic axes (L_1, L_2, L_3) [56Shi].

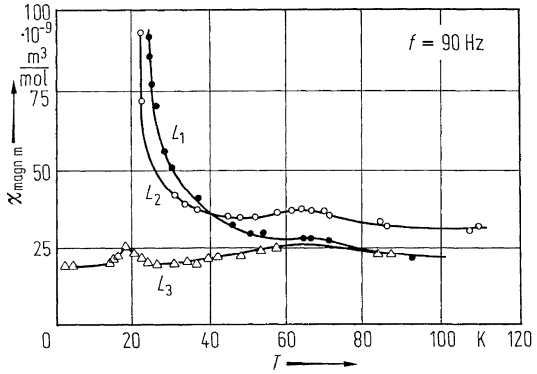

Fig. 52A-1-028. $Cu(HCOO)_2 \cdot 4H_2O$. $\chi_{magn\ m}$ vs. T [63Kob]. $\chi_{magn\ m}$: molar magnetic susceptibilities along the L_1, L_2, and L_3 axes. See Fig. 52A-1-027.

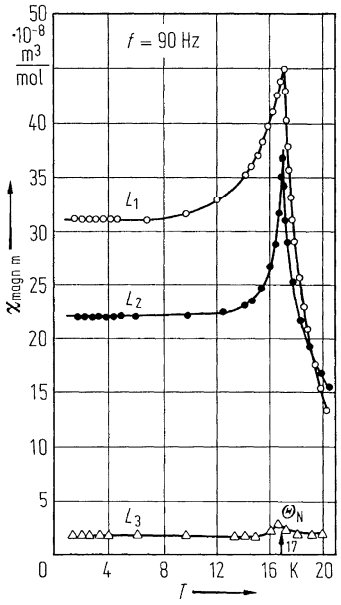

Fig. 52A-1-029. $Cu(HCOO)_2 \cdot 4H_2O$. $\chi_{magn\ m}$ vs. T [63Kob]. $\chi_{magn\ m}$: molar magnetic susceptibilities along the L_1, L_2, and L_3 axes. Θ_N: Néel temperature. See Fig. 52A-1-027.

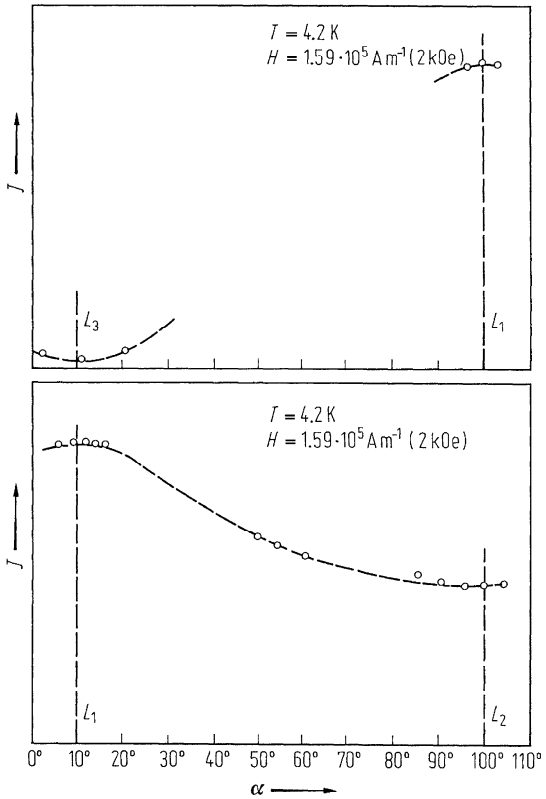

Fig. 52A-1-030. $Cu(HCOO)_2 \cdot 4H_2O$. J vs. α [63Kob]. J: magnetic polarization, α: angle. See Fig. 52A-1-027 for L_1, L_2.

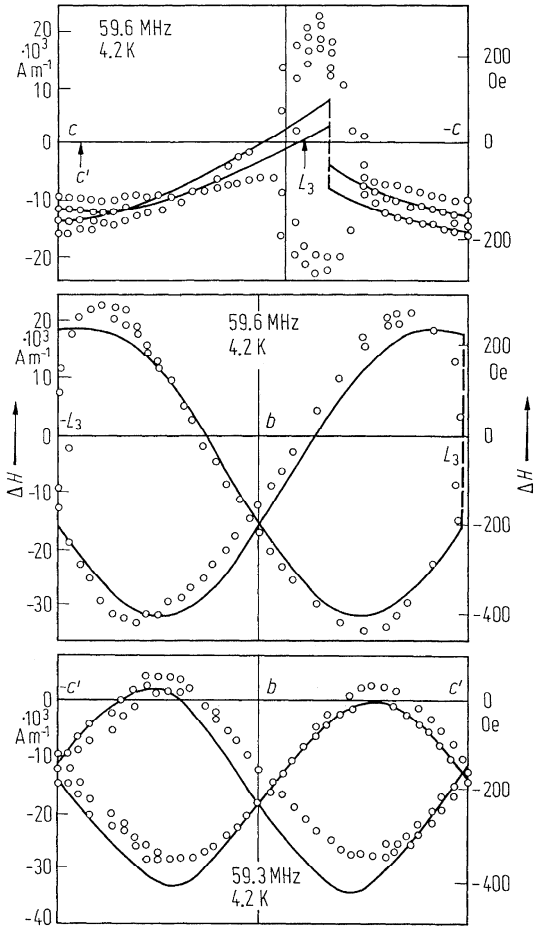

Fig. 52A-1-031. $Cu(HCOO)_2 \cdot 4D_2O$. ΔH vs. rotation angle [71Yam]. ΔH: shift of resonance field from free proton. Circles: experimental results; lines: calculated. c' represents the axis perpendicular to *ab* plane.

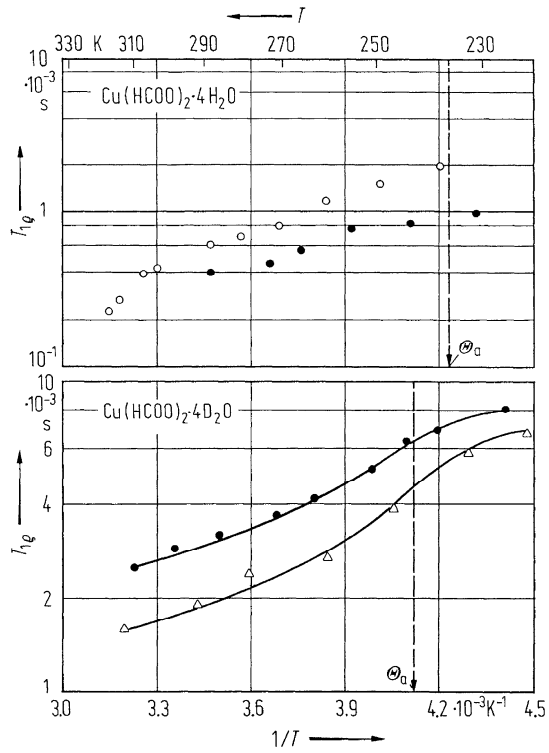

Fig. 52A-1-032. $Cu(HCOO)_2 \cdot 4H_2O$, $Cu(HCOO)_2 \cdot 4D_2O$. $T_{1\rho}$ vs. T^{-1} [74Bon]. $T_{1\rho}$: proton spin-lattice relaxation time in the rotating frame. H_1: r.f. field intensity. Open circles: $H_1 = 3.18 \cdot 10^3$ A m^{-1}; full circles: $H_1 = 1.59 \cdot 10^3$ A m^{-1}; triangles: $H_1 = 0.8 \cdot 10^3$ A m^{-1}.

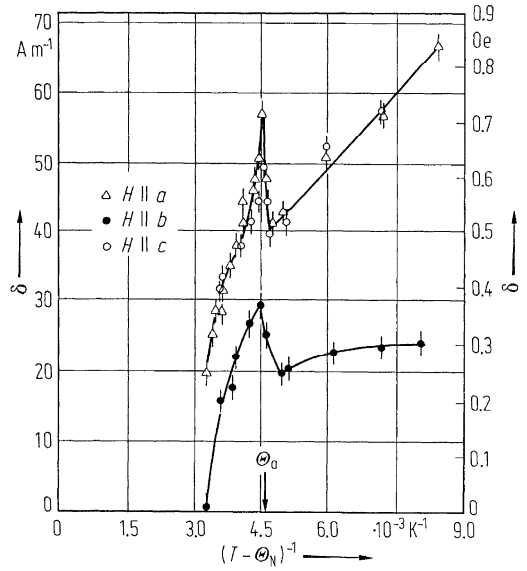

Fig. 52A-1-033. $Cu(HCOO)_2 \cdot 4H_2O$. δ vs. $(T - \Theta_N)^{-1}$ [74Mas]. δ: paramagnetic shift of the formate hydrogen resonance line. $H = 278.5 \cdot 10^3$ A m^{-1}.

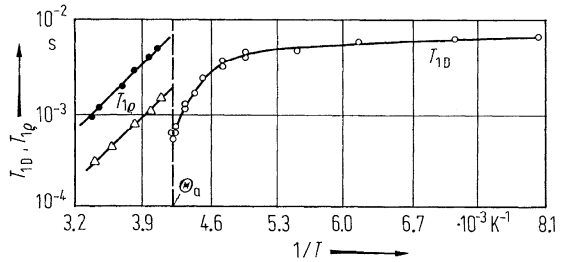

Fig. 52A-1-034. $Cu(HCOO)_2 \cdot 4H_2O$. $T_{1\rho}$, T_{1D} vs. T^{-1} [74Zum]. $T_{1\rho}$: proton spin-lattice relaxation time in the rotating frame. H_1: r.f. field intensity. Full circles: $H_1 = 3.18 \cdot 10^3$ A m^{-1}; triangles: $H_1 = 1.59 \cdot 10^3$ A m^{-1}. T_{1D}: proton spin lattice relaxation time in the dipolar frame.

References

54Kir Kiriyama, R., Ibamoto, H., Matsuo, K.: Acta Crystallogr. **7** (1954) 482.
56Shi Shimada, J., Abe, H., Ono, K.: J. Phys. Soc. Jpn. **11** (1956) 137.
62Ito Itoh, J., Kamiya, Y.: J. Phys. Soc. Jpn. **17** (1962) Suppl. B-I, 512.
62Kir1 Kiriyama, H.: Bull. Chem. Soc. Jpn. **35** (1962) 1199.
62Kir2 Kiriyama, H.: Bull. Chem. Soc. Jpn. **35** (1962) 1205.
62Ska Skalyo, J., Friedberg, S.A.: U. S. Dep. Commun. Office Tech. Serv. AD 285, 553, 1962.
63Kob Kobaysashi, H., Haseda, T.: J. Phys. Soc. Jpn. **18** (1963) 541.
65Oka Okada, K.: Phys. Rev. Lett. **15** (1965) 252.
66Oka Okada, K., Kay, M.I., Cromer, D.T., Almodovar, I.: J. Chem. Phys. **44** (1966) 1648.
67Oka Okada, K.: Phys. Rev. **164** (1967) 683.
67Tub Tuberfield, K.C.: Solid State Commun. **5** (1967) 587.
68See Seehra, M.S., Castner Jr., T.G.: Phys. Kondens. Mater. **7** (1968) 185.
68Seo Seo, I., Kittaka, S., Makita, Y.: Jpn. J. Appl. Phys. **7** (1968) 780.
69Mak Makita, Y., Seo, I.: J. Chem. Phys. **51** (1969) 3058.
69Sod Soda, G., Chiba, T.: J. Phys. Soc. Jpn. **26** (1969) 249.
70Apk Apkar'yants, P.A., Izrailenko, A.N., Sonin, A.S.: Fiz. Tverd. Tela **12** (1970) 3193; Sov. Phys. Solid State (English Transl.) **12** (1971) 2580.
71Bir Bird, M.J., Lomer, T.R.: Acta Crystallogr. Sect. B **27** (1971) 859.
71Yam Yamagata, K., Hayama, M., Odaka, T.: J. Phys. Soc. Jpn. **31** (1971) 1279.
72Hir Hirakawa, K., Hayashi, H., Miike, H.: J. Phys. Soc. Jpn. **32** (1972) 1667.
72Kay Kay, M.I., Kleinberg, R.: Ferroelectrics **4** (1972) 147.
73Can Canterford, R.P., Ninio, F.: J. Phys. C **6** (1973) 575.
73Ges Gesi, K., Ozawa, K.: J. Phys. Soc. Jpn. **35** (1973) 943.
73Kam Kameyama, H., Ishibashi, Y., Takagi, Y.: J. Phys. Soc. Jpn. **35** (1973) 1450.
73Mak Makita, Y., Suzuki, S.: J. Phys. Soc. Jpn. **34** (1973) 278.
74Bon Bonera, G., Massara, C.I., Mognaschi, E.R., Rigamonti, A.: Solid State Commun. **15** (1974) 19.
74Mas Massara, C.I., Mognaschi, E.R.: Ferroelectrics **7** (1974) 115.
74Sas Sasaki, Y.: J. Phys. Soc. Jpn. **37** (1974) 1570.
74Zum Zumer, S., Pirs, J.: Ferroelectrics **7** (1974) 119.
75Kay Kay, M.I.: Ferroelectrics **9** (1975) 171.
75Web Weber, K.E., Flanagan, T.B.: Solid State Commun. **16** (1975) 23.
75Yam Yamamoto, Y., Matsuura, M., Haseda, T.: J. Phys. Soc. Jpn. **38** (1975) 1776.
76Mat Matsuo, T., Kume, Y., Suga, H., Seki, S.: J. Phys. Chem. Solids **37** (1976) 499.
77Fuj Fujimoto, S., Yasuda, N.: Jpn. J. Appl. Phys. **16** (1977) 49.
77Mur Murphy, K.E., Flanagan, B.: J. Chem. Soc., Faraday Trans. I **73** (1977) 1188.
78Ham Hamano, K., Ema, K., Iwane, Y.: J. Phys. Soc. Jpn. **44** (1978) 933.
92Yas Yasuda, N., Suzuki, R.: Ferroelectrics **126** (1992) 127.